Measuring the frequency chirp of white-light continuum in a pump-probe system

A. FALAMAS*, N. TOSA, V. TOSA
National Institute for Research and Development of Isotopic and Molecular Technologies, 67-103 Donat Str, Cluj-Napoca, 400084, Romania

We present here a method which can be used for measuring the instrument response function and the frequency chirp of the white-light continuum (WLC) pulses used in femtosecond time-resolved absorption spectroscopy. The method is based on inducing the optical Kerr effect in different solvents and in the empty quartz cuvette. Additional signal artifacts are observed and identified as the cross phase modulation effect, as well as stimulated Raman. The instrument response function and the dispersion data of the WLC pulse are further used for the study of the electron dynamics in colloidal Au nanoparticles.

(Received September 22, 2016; accepted June 7, 2017)

Keywords: Time-resolved absorption spectroscopy, Instrument response function, White light continuum, Colloidal Au nanoparticles

1. Introduction

In transient absorption (TA) spectroscopy, the molecules from a sample are promoted to an excited state by means of an intense ultrashort pump pulse. A low intensity probe pulse is sent through the sample with a controlled time delay relative to the excitation and the difference between the absorption spectra of the unpumped and the pumped sample is recorded. By changing the time delay between the two pulses, the difference absorption data as a function of time delay and wavelength is obtained. In our case, the time dependent spectral data can give information about the dynamics of the system under study at picosecond time scale. The temporal resolution of such a system is given by the laser pulse duration, the shortest delay between pump and probe beams, the excitation geometry, and the influence of the group velocity dispersion [1].

The white-light continuum (WLC) probe pulses are used in time-resolved absorption spectroscopy for probing the photo-induced transmittance changes. WLC is generated through self-focusing and self phase modulation (SPM) [2, 3] in a nonlinear crystal. SPM leads to an intensity dependent phase shift, which changes the pulse spectrum causing a spectral broadening of the pulse through frequency chirping. The chirp of the WLC results from the generation medium and varies with propagation through lenses, air, the sample cuvette, and influences the dispersion of the TA data. The cross-correlation between the WLC and the pump pulse resulted from measuring an instantaneous signal during TA experiments, determines the instrument response function (IRF) of the system [4]. This function gives the shortest measurable response of a sample and is therefore necessary for accurately measuring the lifetimes of investigated species.

For a proper analysis of the spectra and deconvolution of the kinetic traces it is important to measure the IRF in a given experimental setup and the chirp of the WLC pulse. There are several methods presented in the literature for measuring these parameters, usually based on signal artifacts observed in transient absorption experiments, such as two-photon absorption, stimulated Raman absorption, and cross-phase modulation [5, 6]. The signal has a short duration comparable to the temporal width of the pump-probe cross correlation function and is produced by the simultaneous action of one pump and one probe photon. These artifacts which usually obscure the transient absorption data appear due to the application of very short, intense laser pulses, a spectrally broad probe pulse, and due to the sensitive detection system.

The non-resonant optical Kerr effect (OKE) [7, 8] is another convenient method for measuring the IRF and the frequency chirp of WLC pulse. In OKE experiments an intense, polarized, ultrashort pulse preferentially excites the molecules with transition dipoles oriented along the direction of its electric field. As a result, an anisotropic variation of the polarization is induced in the sample and is detected by the WLC pulse sent with a variable delay. If the pump beam is linearly polarized at 45^o with respect to the probe beam polarized along the x axis, the anisotropic polarization will be different for x and y components [9]. The technique has been used extensively for measuring optical nonlinearities and ultrafast responses of materials [10-15].

In this paper we employ the optical Kerr effect to determine the IRF and to measure the frequency chirp of the WLC pulse in our time-resolved absorption setup. The media we use are different solvents, as well as the empty quartz cuvette. A novelty presented in this work consists of the Raman signal recorded during the OKE experiments and the characterization of the instrumental response

function using this signal, as well. The results are used for processing the time-resolved absorption data acquired from colloidal Au nanoparticles, bare and functionalized with cystine. The frequency chirp of the WLC pulse is used for correcting the dispersion observed in the TA data, while the instrument response function is used to correctly evaluate the electron dynamics in Au colloids.

2. Experimental section

Pulses of 170 fs duration are emitted at 1030 nm wavelength by an Yb:KGW laser (Pharos, Light Conversion) at a repetition frequency of 80 kHz, 75 μJ energy per pulse, and 6 W average power. The main part of the laser pulse is used for pumping a collinear optical parametric amplifier (Orpheus, Light Conversion) yielding tunable output between 620-2600 nm. Additional frequency mixing units can generate second and fourth harmonics of signal and idler beams, extending the total emission range down to 200 nm.

The transient absorption spectrometer (Harpia, Light Conversion, see Figure 1) uses the tunable pump pulses to excite the sample and a white light continuum (WLC) to probe it. The WLC pulse is produced by focusing 10% of the 1030 nm beam into a sapphire crystal of 1 mm thickness. The collimated white light probe pulse is further focused into the sample using an off-axis parabolic reflector, after passing through a neutral density filter. The sample is placed in a quartz cuvette of 1 mm length. The WLC pulse generated here has normal dispersion, meaning that the red wavelengths travel faster than the blue ones. Spectrally, the WLC pulse extends from 480 to 780 nm. The transmitted WLC is detected using a spectrograph with 300 lines/mm grating combined with an array detector.

For the OKE measurements the pump pulse was set at 460 nm with the polarization at 45° relative to the horizontal polarization of the probe beam. A Glan-Thompson polarizer was placed after the Kerr medium so that it allowed a specific polarization to pass and to be detected. The measurements were carried out on different solvents such as water, ethanol, methanol, and the empty quartz cuvette (1 mm length).

Gold colloidal nanoparticles were prepared by photochemical reduction of tetrachloroauric (III) acid (HAuCl4, 99.5%) in water (16.8 mM) with sodium citrate and polystyrene sulfonic acid (PSS). The detailed protocol was presented previously [16]. For the TA measurements 15 μL of $5*10^{-3}$ M cystine solution in water were repeatedly added to 150 μL of Au colloid, until the same amount of ligand and gold colloid was obtained.

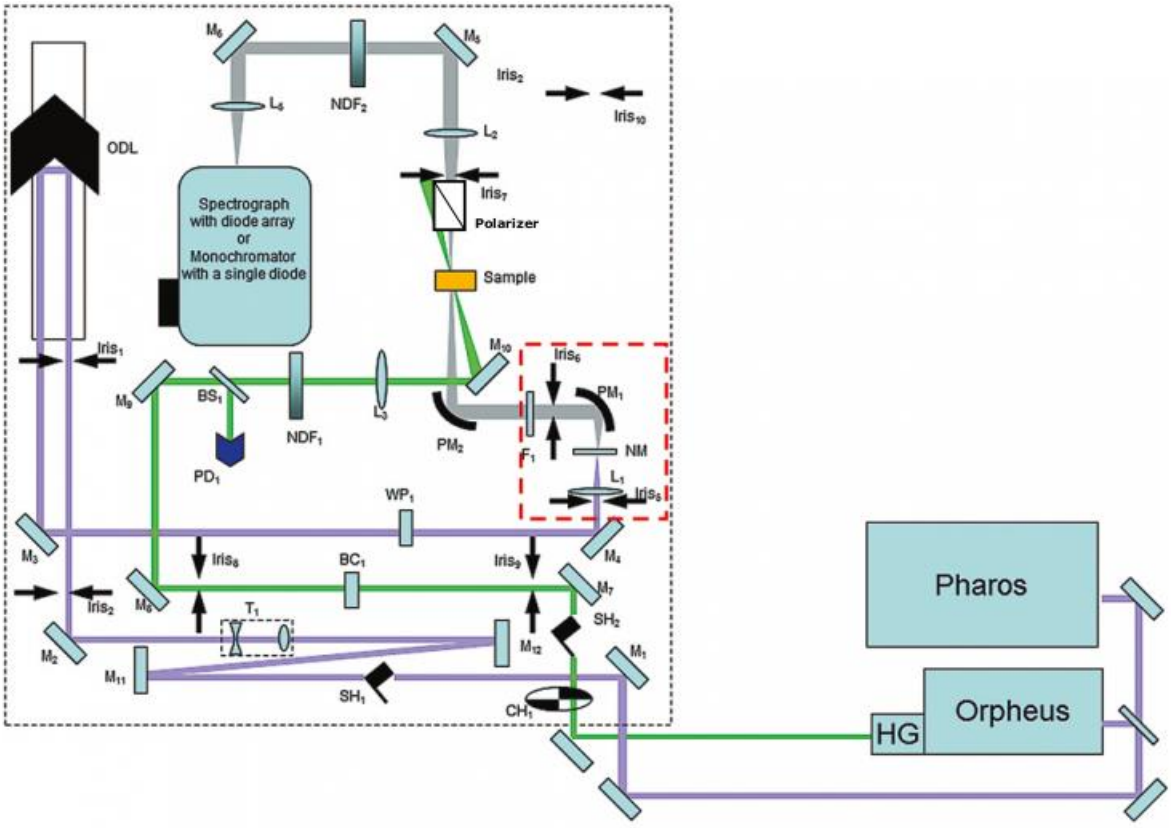

Fig. 1. Schematics of the transient absorption spectrometer showing the Pharos laser used for WLC generation (in the nonlinear medium, NM) and Orpehus used for pumping the sample. The polarizer employed for the OKE experiment was placed after the sample and allowed either the horizontal or the vertical polarization to pass

3. Results and discussions

3.1. Instrument characterization

Fig. 2 presents the transient absorption data recorded in ethanol as a function of wavelength and time delay between pump and probe pulses. The transmitted signal was acquired either when the horizontal (H panel) or the vertical (V panel) polarization was allowed to pass through the polarizer. In the H case we record a superposition between the probe beam and the horizontally polarized signal induced by the pump in the sample. The H case shows well defined oscillatory signals for each wavelength of the white light continuum beam (Fig. $2H_b$). The positive maximum of the signal broadens and shifts towards longer delay times with increasing probe wavelength. A similar situation was observed by Ekvall *et al.* in fused silica plates and the results were reproduced by numerically solving a set of wave propagation equations describing the non-linear coupling between the probe and pump beams. The signal was assigned to the cross phase modulation process [17], which results in a spectral modification in the probe beam due to the temporal changes of the refractive index induced by the intense pump beam. The shifting of the signal towards longer delay times can be assigned to the positive dispersion of the white light continuum beam (red wavelengths travel faster than the blue ones). This means that the overlap between the pump and probe is shifted towards larger delay times for longer wavelengths.

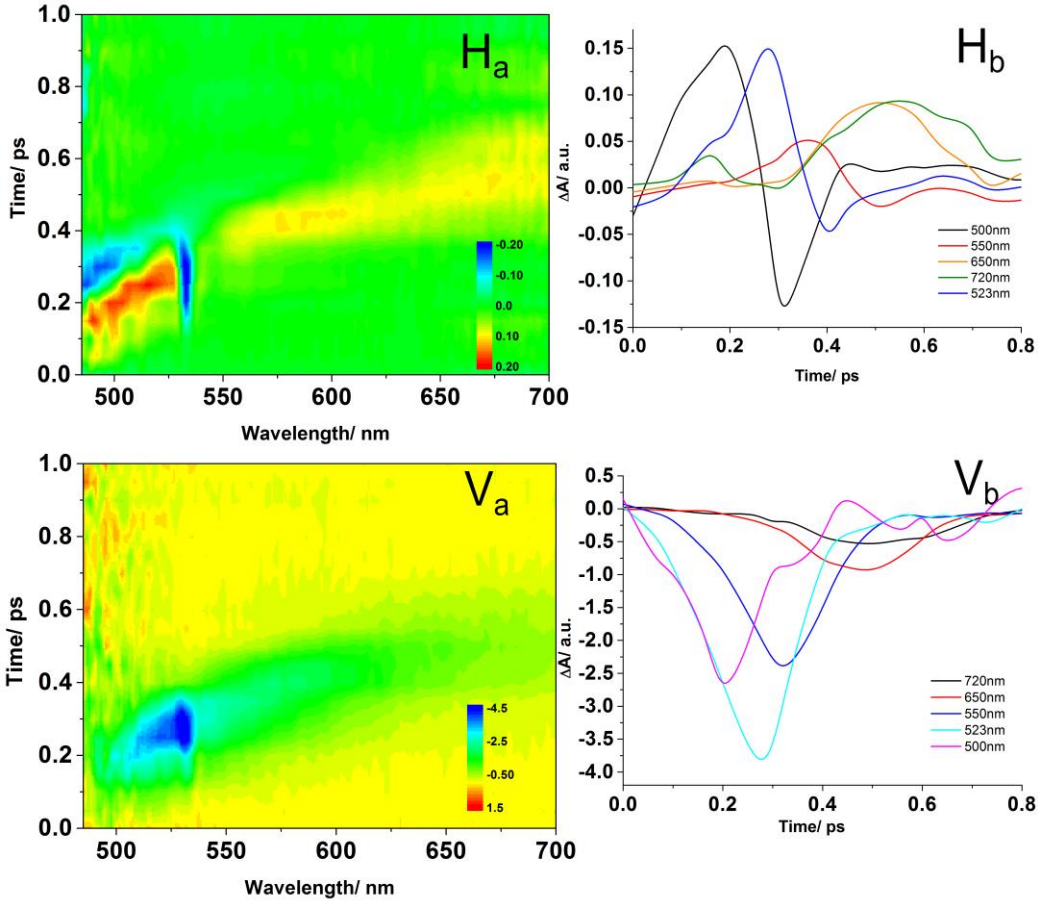

Fig. 2. 3D data carpets and kinetic traces of ethanol recorded in two different geometries of the polarizer: horizontal (Ha and Hb) and respectively vertical (Va and Vb) polarization is transmitted. Pump beam was set at 460 nm

The V case, on the other hand, corresponds to the OKE signal and shows only the vertically polarized signal induced by the pump and detected by the probe beam. The negative sign of the signal seen in Fig. $2V_b$ is due to the method used for calculating the difference absorption spectra:

$$\Delta OD(t,\lambda) = \lg \frac{I_{unpumped}(\lambda)}{I_{pumped}(t,\lambda)} 0 - I_{pr-y} < 0\,, \qquad (1)$$

where $I_{pr\text{-}y}$ is the intensity of the probe signal induced by the pump beam along the *y* direction.

The associated spectra for ethanol and the empty quartz cuvette recorded at different time delays in the H configuration of the Glan Thompson polarizer are presented in Fig. 3. The spectra show a broad peak which shifts to longer wavelengths with increasing the delay times between pump and probe beams, due to the positive chirp of the WLC beam. In both cases, the entire process lasts ~0.6 ps.

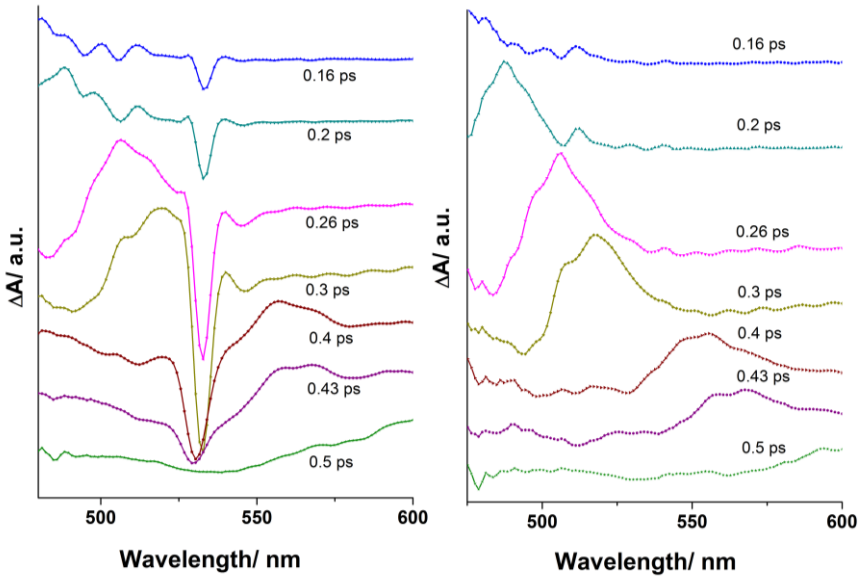

Fig. 3. Time-resolved spectra of ethanol (left) and the quartz cuvette (right), recorded when pump beam was set at 460 nm. Time delays are indicated in the figure

We observe also a stimulated Raman amplification signal which appears as a sharp, negative peak at 531 nm in the spectra acquired from ethanol (Fig. 3 left). This peak corresponds to the Raman band assigned to CH_3 and CH_2 stretching vibrations [18]. The spectral width of this peak is ~185 cm^{-1}, meaning that it might encompass all of the CH_2 and CH_3 symmetric and antisymmetric stretching vibrations of ethanol present in the 2880-3020 cm^{-1} spectral range [18]. The Raman band appears as a negative signal in both H and V configurations and can be explained as follows: the pump pulse excites the molecules to a virtual state, which is a very short lived distortion of the electron cloud caused by the oscillating electric field of the light. The molecules relax back to a higher vibrational level so that when the probe pulse passes through the sample its absorption will be lower. The probe pulse sees the gap in the ground state at the frequency corresponding to the emitted Raman photon. The Raman photons are scattered into the probe pulse which carries a negative ΔOD signal, as if emission took place [19].

The Raman band is recorded at the corresponding wavelength for each of the investigated solvents. When pumping the ethanol molecules with 460 nm the Raman band is observed at 531 nm and shifts accordingly to 494 nm when pumped with 430 nm (see Table 1). On the other hand, in the spectra recorded in water pumped at 460 nm, the peak is observed at 545 nm and is assigned to OH stretching vibrations. Moreover, when a mixture of both ethanol and water was used, both Raman bands were observed at 531 and 545 nm, respectively (not shown here). Furthermore, when the signal is recorded for the empty quartz cuvette, no Raman bands are observed (Fig. 3 right). The reproducibility of this signal, its amplitude, and appearance around time zero, make it convenient for the identification of the temporal resolution of the system. We calculated the duration of the Raman signal for the water experiment and obtained a value of ~0.195 ps, which is close to the duration of our laser pulse.

These results pave the way for further experiments towards ultrafast vibrational dynamics [20] in order to extract information about the phase and amplitudes of low-frequency modes excited using the 170 fs duration laser pulse in our laboratory. A feasible way for doing this, which we intend to further develop, would be to functionalize colloidal nanoparticles with a dye, which exhibits low-frequency modes that can be observed when excited with femtosecond laser pulses.

Table 1. Pump wavelengths and the shift observed for the Raman bands for each of the analyzed solvents

Solvent	**λ_{pump} (nm)**	**λ_{Raman} (nm)**	**Vibrational assignment**
Methanol	450	521	$\nu(CH_3)$, $\nu(CH_2)$
Methanol	460	531	$\nu(CH_3)$, $\nu(CH_2)$
Ethanol	430	494	$\nu(CH_3)$, $\nu(CH_2)$
Ethanol	460	531	$\nu(CH_3)$, $\nu(CH_2)$
Water	460	545	ν(OH)
water	480	574	ν(OH)

To determine the temporal response of our pump-probe system, several kinetic traces were selected from both the water and ethanol OKE measurements (V case). As expected, all of the curves are nearly symmetric and can be obtained with a Gaussian fit (see Fig. 4). The instrument response function was determined from the FWHM of the Gaussian peak. The IRF values are very similar for all the kinetic traces and they average to 200 fs for both water and ethanol.

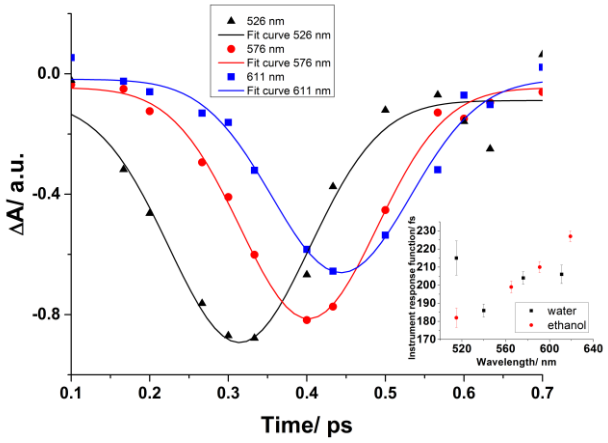

Fig. 4. OKE kinetic traces observed at different wavelengths of the probe beam and their Gaussian fit. The experiment was performed in water with the pump beam set at 460 nm. The inset shows the resulted IRF values for water and ethanol at different probe wavelengths

The TA experiments exhibit a strong wavelength dependency of the trace of time zero points on a sub-picosecond time scale (see Fig. 5). The signal appears earlier at shorter wavelengths than at longer ones and this temporal evolution is a trace of the frequency chirp of the white light continuum components. Therefore, the TA data need to be corrected for the dispersion of the WLC pulse before any other analysis, in order to synchronize the time zero for all wavelengths. To measure the frequency chirp structure of the WLC, the OKE signal's maximum at different wavelengths across the probe pulse spectral range was fitted with a second order polynomial function. The results obtained for the OKE experiments in water and ethanol using the pump set at 460 nm are shown in Fig. 5A. The break in the data corresponds to the location of the Raman band, which was excluded from these measurements. The vertical time shift between the data is related to the experimental conditions and the selected time zero between pump and probe pulses. The polynomial coefficients resulted from fitting this data, which are given in Eq. 2, were successfully used for correcting the dispersion in the transient absorption measurements on Au nanoparticles, obtained in similar conditions (Fig. 5B and C). We did not include a calculation for the group velocity dispersion (GVD) of the probe pulse in the sample, as we determined the GVD for quartz using the Sellmeier coefficients and observed that the time delay due to dispersion between the blue and red wavelengths extremities of our WLC pulse is on the order of a few tens of fs, meaning that it plays a minor role in our data.

$$t_{water} = 0.39 + 0.0036 \cdot \lambda + 7.77e^{-6} \cdot \lambda^2$$
$$t_{ethanol} = 0.177 + 0.0034 \cdot \lambda + 6.87e^{-6} \cdot \lambda^2 \quad (2)$$

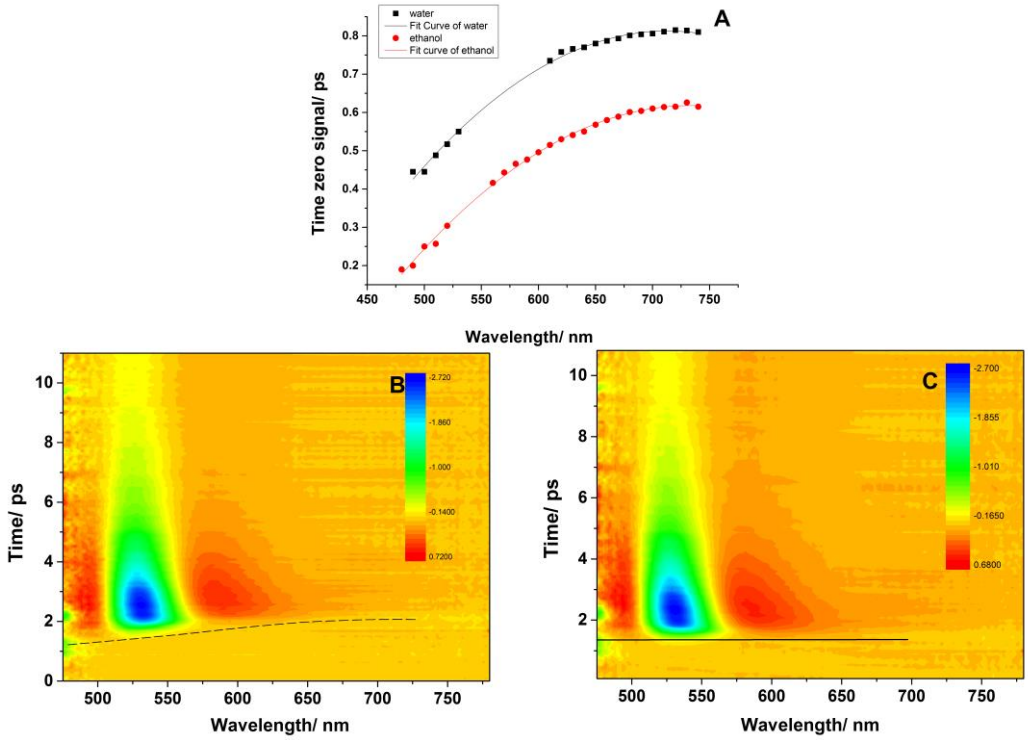

Fig. 5. Wavelength dependence of the time zero delay in the white light probe beam determined using the OKE technique in water and ethanol (A). Image of the raw TA data collected from colloidal Au nanoparticles (B) and image of the dispersion corrected data (C), showing the time zero synchronization for all wavelengths

3.2. Ultrafast dynamics of colloidal Au nanoparticles

The obtained instrument response function and dispersion coefficients values were further used for probing the ultrafast dynamics of colloidal Au nanoparticles bare and functionalized with cystine. In a previous paper [16], the data on IRF and WLC dispersion were not available so we fitted the kinetic traces with a double exponential model. We found that the relaxation mechanism of the "hot" electrons in Au nanoparticles show a fast component of ~1 ps and a slower one of ~300 ps. We assumed that the laser pulse excites the electrons in the Au nanoparticles to states above the Fermi level inducing a highly nonthermal electron distribution. The electron gas cools down through electron-phonon coupling and phonon-phonon interactions with the surrounding medium, causing the excited electrons above the Fermi level to lose energy. As a consequence, the temperature decreases and the system returns to ground state [19].

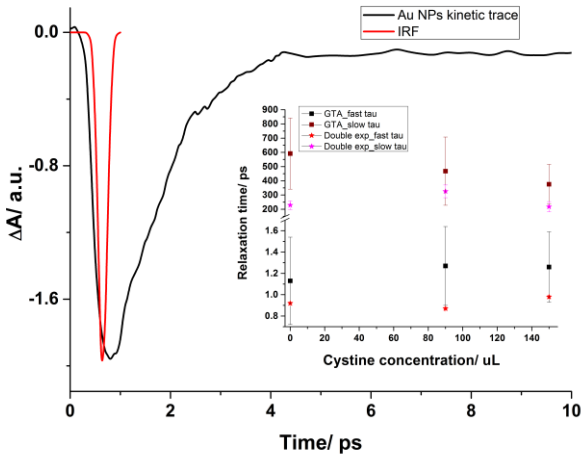

Fig. 6 The instrument response function overlapped with a kinetic trace characteristic to the Au nanoparticles functionalized with cystine. In the inset: the fast and long decay times of electrons in colloidal Au nanoparticles pumped with 440 nm and obtained either using Global Target Analysis or by fitting the kinetic traces with a double exponential function

Here we employ Global Target Analysis (GTA) to study the electron dynamics, which considers discreet compartments connected by rate equations [21, 22]. The pump pulse excites the population in one or several compartments and it is transferred from one compartment to another according to the chosen connectivity scheme. Having a priori knowledge of the kinetics of the colloidal Au nanoparticles we can employ GTA to describe the concentrations of the compartments as it follows:

$$\frac{dc_1(t)}{dt} = I(t) - \frac{1}{\tau_1} c_1(t)$$
$$\frac{dc_2(t)}{dt} = \frac{1}{\tau_1} c_1(t) - \frac{1}{\tau_2} c_2(t) \quad (3)$$

We assume that the pump pulse *I(t)*, a quantity proportional to the instrument response function, excites the population to a first compartment. From the first compartment the population (c_1) is transferred to a second one with the characteristic time τ_1 corresponding to electron-phonon couplings. The population (c_2) returns to the ground state with the characteristic time τ_2 corresponding to phonon-phonon interactions.

The data pre-processing consisted of calibrating the wavelengths with a holmium oxide reference and of correcting the dispersion. The TA data carpets before and after calibration are shown in Fig. 5 (B and C). The instrument response value obtained for water (0.200 ps) was kept constant throughout the fitting. After the dispersion correction, the time zero is synchronized for all wavelengths. Fig. 6 shows the fast and slow decay times of the "hot" electrons in Au nanoparticles bare and functionalized with increasing concentrations of cystine compared to the values obtained when the kinetic traces were fitted with a double exponential function [16]. The fast decay times obtained using GTA are higher than the ones resulted when the fit was performed using a double exponential function. This fact can be assigned to the fitting method using the double exponential function and the fact that at that time the instrument response function was unknown. The resulted fast decay times are similar for bare and functionalized Au nanoparticles with different concentrations of cystine. This could be assigned to the fact that this decay time is characteristic to the electron-phonon coupling which is influenced mostly by the Au nanoparticles and less by the molecules adsorbed on the Au nano-surface. On the other hand, the slow decay times show similar values for both fitting methods, as they are less influenced by the IRF. Additionally, a small decrease of the slow decay times with increasing the ligand concentration is observed when using GTA. We assume that a higher concentration of the ligands adsorbed on the Au nanoparticles surface increases the coupling of the nanoparticles with the medium; therefore more de-excitation paths are available.

4. Conclusions

We measured the instrument response function and the frequency chirp of the white light continuum in our pump-probe system. For this we used the non-resonant optical Kerr effect taking into account the additional signal artifacts observed in TA data. The instrument response function of the system was measured in both ethanol and water and similar values were obtained. The frequency chirp structure of the WLC beam was determined by fitting with a second order polynomial function the OKE signal maxima obtained for each solvent. The coefficients were used for correcting the dispersion observed in TA data. The instrument response function was used when Global Target Analysis was applied to the data obtained on colloidal Au nanoparticles for the evaluation of the electron dynamics.

Acknowledgements

We thank Mikas Vengris for several illuminating discussions. A.F. and V.T. acknowledge financial support from a grant of the Romanian National Authority for Scientific Research and Innovation, CNCS-UEFISCDI, project no. PN-II-RU-TE-2014-4-0425. N.T. acknowledges financial support from Project 03ELI-ProPW.

References

[1] M. Lorenc, M. Ziolek, R. Naskrecki, J. Karolczak, J. Kubicki, A. Maciejewski, Appl. Phys. B **74**, 19 (2002).
[2] A. Brodeur, S. L. Chin, Journal of the Optical Society of America B **16**, 637 (1999).
[3] R. L. Fork, C. V. Shank, C. Ifirlimann, R. Yen, W. J. Tomlinson, Optics Lett. **8**, 1 (1983).
[4] M. Ziolek, M. Lorenc, R. Naskrecki, Appl. Phys. B **72**, 843 (2001).
[5] A. Maciejewski, R. Naskrecki, M. Lorenc, M. Ziolek, J. Karolczak, J. Kubicki, M. Matysiak, M. Szymanski, J. Mol. Struc. **555,** 1 (2000).
[6] S. A. Kovalenko, A. L. Dobryakov, J. Ruthmann, N. P. Ernsting, Phys. Rev. A **59,** 35 (1999).
[7] S. Yamaguchi, H. Hamaguchi, Appl. Spectrosc. **49**, 1513 (1995).
[8] Y. Wu, Z. Wang, X. Zhang, W. Li, L. Huang, W. Li, Q. Wu, J. Xu, Optics Express **22,** 2879 (2014).
[9] P. Bartolini, A. Taschin, R. Eramo, R. Torre, Time-resolved experiments in complex liquids - an experimental perspective, Ed. R. Torre (Springer, 2008) p. 73.
[10] W. Tan, H. Liu, J. Si, X. Hou, Appl. Phys. Lett. **93,** 051109 (2008).
[11] H. Zhang, Z. Zhou, A. Lin, J. Cheng, H. Liu, J. Si, F. Chen, X. Hou, J. Opt. **14,** 065201 (2012).
[12] H. Liu, W. Tan, J. Si, X. Liu, X. Hou, Opt. Express **16,** 13486 (2008).
[13] R. A. Negres, J. M. Hales, A. Kobyakov, D. J. Hagan, E. W. Van Stryland, IEEE J. Quantum Electronics **38,** 1205 (2002).
[14] P. Bejot, Y. Petit, L. Bonacina, J. Kasparian, M. Moret, J.-P. Wolf, Opt. Express **16,** 7564 (2008).
[15] D. McMorrow, W. T. Lotshaw, G. A. Kenney-Wallace, IEEE J. Quantum Electronics **24,** 443 (1988).
[16] A. Falamas, N. Tosa, V. Tosa, J. Quant. Spectr. Rad. Transfer **162**, 207 (2015).
[17] K. Ekvall, P. van der Meulen, C. Dhollande, L.-E. Berg, S. Pommeret, R. Naskrecki, J.-C. Mialocq, J. Appl. Phys. **87**, 2340 (2000).
[18] Y. Yu, K. Lin, X. Zhou, H. Wang, S. Liu, X. M. Hefei, J. Phys. Chem. C **11,** 8971 (2007).
[19] S. Link, M. A. El-Sayed, Annu. Rev. Phys. Chem. **54,** 331 (2003).
[20] J. P. Kraack, A. Wand, T. Buckup, M. Motzkusa, S. Ruhman, Phys. Chem. Chem. Phys. **13,** 14487 (2013)
[21] C. Ruckebusch, M. Sliwa, P. Pernot, A. de Juan, R. Tauler, R., J. Photochem. Photobiol. C: Photochem. Rev. **13,** 1 (2012).
[22] Ivo H.M. van Stokkum, D.S. Larsen, R. van Grondelle, Biochem. Biophys. Acta **1657**, 82 (2004).

*Corresponding author: afalamas@gmail.com